Supporting Information

Tuning of Conformational Dynamics Through Evolution-Based Design Modulates the Catalytic Adaptability of an Extremophilic Kinase

Ricardo A. Zamora†¶, Cesar A. Ramirez-Sarmiento‡, Víctor Castro-Fernández†, Pablo Villalobos†, Pablo Maturana†, Alejandra Herrera-Morande†, Elizabeth A. Komives§, Victoria Guixé†*.*

† Departamento de Biología, Facultad de Ciencias, Universidad de Chile. Las Palmeras 3425, Ñuñoa, Santiago, Chile.
‡ Instituto de Ingeniería Biológica y Medica, Escuela de Ingeniería, Medicina y Ciencias Biológicas, Pontificia Universidad Católica de Chile. Avenida Vicuña Mackenna 4860, Macul, Santiago, Chile.
§ Department of Chemistry and Biochemistry, University of California, San Diego, La Jolla, California, 92092-0378.

¶ Present Address: Institute for Bioengineering of Catalonia (IBEC), Carrer de Baldiri Reixac 15-21, 08028 Barcelona, Spain. E-mail: rzamora@ibecbarcelona.eu

*Address correspondence to:

Victoria Guixé

Phone: + 56 2 22978 7335

E-mail: vguixe@uchile.cl

Elizabeth A. Komives

Phone: 858-534-3058

E-mail: ekomives@ucsd.edu

Contents of the material supplied as Supporting Information.

1. Supporting experimental procedures:

a) Enzyme expression, purification and mutagenesis
b) Characterization of ADP-dependent phosphofructokinase activity
c) Hydrogen-deuterium exchange mass spectrometry (HDXMS)
d) Analysis of melting temperature (Tm)
e) Molecular modelling
f) Molecular dynamics simulations and principal component analysis

2. Supporting Results:

a) Table S1. Structural comparison between the psychrophilic *Mb*PFK/GK and the mesophilic *Mm*PFK/GK homology models.
b) Table S2. Kinetic parameters for the psychrophilic *Mb*PFK/GK and the mesophilic *Mm*PFK/GK at different temperatures.
c) Table S3. Thermodynamic activation parameters for the psychrophilic *Mb*PFK/GK and the mesophilic *Mm*PFK/GK at different temperatures.
d) Table S4. Thermodynamic parameters for the temperature-dependent interaction of F6P with the active site of the psychrophilic *Mb*PFK/GK, the mesophilic *Mm*PFK/GK, the psychrophilic *Mb*PFK/GK quadruple mutant and the psychrophilic *Mb*PFK/GK double mutant.
e) Table S5. Amino acid residues of the active site of the psychrophilic *Mb*PFK/GK and the mesophilic *Mm*PFK/GK (5Å).
f) Table S6. Sequences of the 35 selected residues from the HDXMS experiments in the psychrophilic *Mb*PFK/GK.
g) Table S7. Sequences of the 35 selected residues from HDXMS experiments in the mesophilic *Mm*PFK/GK.
h) Table S8. Sequences of the 35 selected residues from HDXMS experiments in the psychrophilic *Mb*PFK/GK quadruple mutant.
i) Figure S1. Raw data of the thermal unfolding of the psychrophilic *Mb*PFK/GK and the mesophilic *Mm*PFK/GK recorded by circular dichroism following the signal at 220 nm.

j) Figure S2. Average of the normalized deuterium uptake (amides) for all residues shown in Figure 2 from the psychrophilic *Mb*PFK/GK and the mesophilic *Mm*PFK/GK.
k) Figure S3. Structure-based multiple sequence alignment of extant and ancestral ADP-dependent kinases.
l) Figure S4. Deuterium uptake plots of the psychrophilic *Mb*PFK/GK residues used in the HDXMS data analysis presented in Figure 2A.
m) Figure S5. Deuterium uptake plots of the mesophilic *Mm*PFK/GK residues used in the HDXMS data analysis presented in Figure 2B.
n) Figure S6. Comparison of the H/D exchange kinetics of residues involved in the intradomain (A) and interdomain (B) interactions in the psychrophilic *Mb*PFK/GK (blue blocks) and the mesophilic *Mm*PFK/GK (red blocks) at 10 °C, 25 °C, and 40 °C.
o) Figure S7. Representation of the trajectories obtained from the principal component analysis for the psychrophilic *Mb*PFK/GK, mesophilic *Mm*PFK/GK, and psychrophilic *Mb*PFK/GK quadruple mutant.
p) Figure S8. Deuterium uptake plots of the psychrophilic *Mb*PFK/GK quadruple mutant residues used in the HDXMS data analysis presented in Figure 6D.
q) Figure S9. Comparison of the H/D exchange kinetics of the residues involved in the intradomain (A) and interdomain (B) interactions in the psychrophilic *Mb*PFK/GK (blue blocks) and the psychrophilic *Mb*PFK/GK quadruple mutant (cyan blocks) at 25 °C.
r) Figure S10. SDS-PAGE of the purification of the wild type and mutants ADP-dependent sugar kinases.

Supporting experimental procedures

Enzyme expression, purification and mutagenesis

The genes for ADP-PFK/GK from *M. burtonii* (*Mb*PFK/GK, Uniprot: Q12WB9) and *M. maripaudis* (*Mm*PFK/GK, Uniprot: A4FWN8) were synthesized by Genscript (Piscataway, NJ, USA) and optimized for expression in *E. coli.* Both genes were directly cloned into the modified pET-28b vector in the restriction sites *NdeI* and *BamHI*, which inserted an N-terminal hexahistidine tag joined to a TEV protease recognition site. *E. coli* strain BL21(DE3) was transformed with ADP-PFK/GK from *M. burtonii* plasmid and *E. coli* BL21(DE3) pLysS was transformed with ADP-PFK/GK from *M. maripaludis* plasmid. For the ADP-PFK/GK from *M. burtonii* the cells were cultured at 37 °C in LB broth containing 35 $\mu g \cdot mL^{-1}$ kanamycin and grown until OD_{600} of

approximately 1.0. For the ADP-PFK/GK from *M. maripaludis* the cells were cultured at 37 °C in LB broth containing 35 $\mu g \cdot mL^{-1}$ kanamycin and 35 $\mu g \cdot mL^{-1}$ chloramphenicol and grown until OD_{600} of approximately 0.4. For both enzymes the protein expression was induced by adding 1 mM of isopropyl-β-D-thiogalactopyranoside. Then, cultures were incubated at 14 °C overnight for ADP-PFK/GK from *M. burtonii* and at 30 °C for ADP-PFK/GK from *M. maripaludis.* For purification, cells were collected by centrifugation, suspended in binding buffer (25 mM Tris-HCl pH 7.8, 500 mM NaCl, 20 mM imidazole and 5 mM $MgCl_2$) and disrupted by sonication. After centrifugation (18514 x g for 20 min, at 4 °C) the soluble fraction was loaded onto a Ni^{+2}-NTA affinity column (HisTrap HP, GE Healthare, UK) and protein eluted with a linear gradient of imidazole between 20 and 500 mM. Fractions with PFK-ADP activity were pooled, concentrated, dialyzed against binding buffer and stored at 4 °C. Enzyme purity was analyzed by SDS-PAGE stained with Coomassie blue (Figure S10). The psychrophilic *Mb*PFK/GK mutants were obtained by site-directed mutagenesis of specific amino acid residues, and mutated residues were verified by sequencing.

Characterization of ADP-dependent phosphofructokinase activity S4

Phosphofructokinase ADP-dependent activity was assayed as previously described in Zamora et al[1]. The ADP-dependent PFK activity (EC 2.7.1.146) was determined spectrophotometrically in a continuous assay monitoring NADH oxidation at 340 nm coupled to the fructose 1,6-biphosphate production. The standard assay reaction was carried out in a final volume of 0.5 mL and contained Pipes buffer 25 mM pH 6.5, NADH 0.2 mM, 5 U of α-glycerophosphate dehydrogenase, 50 U of triosephosphate

isomerase and 1.3 U of aldolase as auxiliary enzymes and variable concentrations of glucose and MgADP. Kinetic experiments were performed at different temperatures using a Hewlett Packard 8453 spectrophotometer. Initial rates were determined from the change in NADH concentration, calculated using an extinction coefficient of 6.22 $mM^{-1}cm^{-1}$. An enzyme unit is defined as the conversion of 1 µmol of product per minute. The kinetic parameters were determined varying the concentration of substrates at saturating co-substrate concentration. In each case, $MgCl_2$ 5 mM in excess over the ADP concentration was used. Initial velocity studies were performed in triplicate. Data were analyzed using nonlinear regression and fitted to the Michaelis-Menten equation.

Hydrogen-deuterium exchange mass spectrometry (HDXMS)

HDXMS measurements were performed using a Synapt G2Si system (Waters Corporation). Deuterium exchange reactions were carried out by a Leap HDX PAL autosampler (Leap Technologies, Carrboro, NC). For digestion test, the enzymes were injected into a column containing protease pepsin immobilized in agarose. To optimize the peptide identification process, the concentration used was 15 µM. The peptides obtained were identified using the software ProteinLynx Global SERVER PLGS 3.0 (Waters corporation), considering only the peptides that had a score greater than 7, an abundance of at least 3 ppm and that these could be identifiable in at least two of the three experiments made. Once the peptides were identified, the HDXMS experiments were performed in EX2 conditions. Independent HDXMS experiments for each enzyme were carried out in triplicate using buffer 25 mM Pipes, pH 6.5 in D_2O. The enzyme concentration used for all HDXMS

experiments were 5 µM. In all experiments, 5 µL of each enzyme were diluted in 55 µL of deuterated water (D_2O) at incubation times of 0, 0.5, 1, 2, 5, 10 and 30 minutes at 10°C, 25°C and 40°C. To quench the deuterium exchange reactions, an equivalent volume to that of the reaction mixture composed of Guanidinium Chloride (Gnd-HCl) 2 M and 1% formic acid, pH 2.66 was added. The samples were then injected into a column containing protease pepsin immobilized in agarose and kept there for 2 minutes at 1°C. The peptides resulting from the proteolysis were separated by chromatography using a mobile phase of formic acid 0.1% and a gradient of 7% to 95% acetonitrile for 7 minutes and analyzed in a Waters Synapt G2Si quadrupole time-of-flight mass spectrometer following electrospray injection. Continuous lock mass correction was accomplished with infusion of leu-enkephalin (m/z = 556.277) every 30 s (mass accuracy of 1 ppm for calibration standard. The quantification of the hydrogen-deuterium exchange of each peptide was performed using the DynamX 3.0 software (Waters Corporation). The units used for the quantification were Dalton (Da).

For the psychrophilic *Mb*PFK/GK, 142 peptides were identified and 35 of these peptides were used to perform the analyzes (Table S6, Figure S4). The selected peptides for analysis have an 89.8% of coverage with 1% of redundancy. For the mesophilic *Mm*PFK/GK, 134 peptides were identified and 35 of these peptides were used to perform the analyzes (Table S7, Figure S5). The selected peptides for analysis have an 87.8% of coverage with 1% of redundancy. Finally, for the psychrophilic *Mb*PFK/GK quadruple mutant, 115 peptides were identified and 34 of these peptides were used to perform the analyzes (Table S8 Figure S8). The selected peptides for analysis have an 88.9% of coverage with 1% of redundancy. All the selected

peptides analyzed were present at least in two HDXMS experiments for each enzyme. The deuterium uptake of all the peptides analyzed was corrected for back-exchange (~31%, ~27%, ~29% for the psychrophilic *Mb*PFK/GK, the mesophilic *Mm*PFK and the psychrophilic *Mb*PFK/GK quadruple mutant, respectively), based on a full-deuteration controls.

Analysis of melting temperature (Tm)

Thermal unfolding curves for the ADP-dependent enzymes were obtained by circular dichroism. The heat-induced unfolding spectra were obtained in a JASCO J-1500 spectropolarimeter coupled to a Peltier system for temperature control, using a constant flow of nitrogen. Measurements were performed following the dichroic signal at 222 nm, with a bandwidth of 1nm and an integration time of 16 seconds. The conditions in employed were: 25 mM PIPES buffer pH 6.5, $MgCl_2$ 5 mM and NaCl 500 mM.

Molecular modelling

The homology model of the ancestor MMT was built using the methodology described in Zamora et al[1]. Briefly, the *Pyrococcus furiosus* glucokinase structure in its closed conformation (PDBiD: 1U4A) and the *Pyrococcus horikoshii* phosphofructokinase structure in its open conformation (PDBiD: 1U2X) were used as templates. The structure of phosphofructokinase in the open conformation was split off, and the structures of the major and minor domains of this enzyme were structurally and independently aligned with the *P. furiosus* glucokinase structure. Subsequently, with the structural templates of both enzymes in its closed conformation, fifty models were built using

MODELLER 8[2]. The best potential DOPE model was chosen. Quality of the best model was evaluated with ProSA[3] and VERIFY3D[4].

Molecular dynamics simulations and principal component analysis

Homology models used for the molecular dynamics simulations were obtained from previous publications[1,5]. Molecular dynamics simulations were performed using the NAMD 2.13 CUDA implementation[6] and the CHARMM36m force field[7]. Each homology model was placed in a water box and the system neutralized with NaCl. The energy minimization of the systems was done using iterations with no imposing restrictions. The systems were equilibrated by 20 ns after which the molecular dynamics simulations were extended by other 210 ns of production. The assembly used to carry out the molecular dynamics simulations was NTP, setting the system temperature at 298K and pressure at 1 atmosphere. The time step was 2 fs. For every system, molecular dynamics simulation was performed in triplicate with different random seed.

To identify correlated movements of functional significance, a principal component analysis (PCA) was performed. From the trajectories, a new file containing only the coordinates of the alpha-carbons of each residue for each protein was generated. In each of these files, all the rotation and translation movements were suppressed by the superimposition of each frame of the simulation. With these new trajectories, the principal components were analyzed using the Carma program[8]. This analysis generates a set of eigenvectors and eigenvalues which allow to dissect the different modes of movements or principal components (PC) from the conformational space explored during the trajectory. The eigenvectors or

principal components represent a correlated displacement of the protein residues, and each eigenvalue represents the amplitude of this movement. To describe the main components of the movements, each eigenvector is ordered in decreasing order according to its own values. If only a few significant components are needed to explain most of the variance of the system, the movements are highly correlated or collective. On the contrary, if many major components are required to describe the total variance, the movements are random. The analysis done in the *Carma* program allows obtaining the movement described by each eigenvector in a trajectory file which was visualized and analyzed using VMD 1.9.3[9].

Supporting Results

Table S1.

	***Mb*PFK/GK**	***Mm*PFK/GK**
Nro. of residues	485	463
Molecular mass (Da)	54,168	52,701
Residue Identity[a]	33%	
Secondary Structure[b]		
Helix	40%	40%
Beta	24%	25%
Turn	20%	19%
Coil	35%	34%
Total ASA ($Å^2$)[b]	22900.8	22019.5
ASA Backbone ($Å^2$)[b]	2406.6	2128.2
ASA sidechain ($Å^2$)[b]	20494.2	19891.3
Fraction nonpolar ASA[b]	0.55	0.58
Fraction polar ASA[b]	0.20	0.20
Fraction charged ASA[b]	0.25	0.22
Intraprotein interactions		
Van der Waals total[c]	432	415
SC-MC[c]	38	27
MC-SC[c]	55	60
SC-SC[c]	339	328
H-bonds total[c]	425	423
MC-MC[c]	324	299
MC-SC[c]	40	40
SC_MC[c]	15	22
SC-SC[c]	46	62
Ionic[c]	17	29
π- π stack[c]	10	13
π-cation[c]	2	0

Structural comparison between the psychrophilic *Mb*PFK/GK and the mesophilic *Mm*PFK/GK homology models.

a. VMD (Version 1.9.3)[9]
b. Vadar server (Version 1.8)[10]
c. Ring server (Version 2.0)[11]

Table S2. Kinetic parameters for the psychrophilic *Mb*PFK/GK and the mesophilic *Mm*PFK/GK at different temperatures.

Enzyme	T, °C	K_m, μM	k_{cat}, s^{-1}	k_{cat}/K_m, $M^{-1}s^{-1}$
***Mb*PFK/GK**	10	13 ± 5	2.3 ± 0.2	1.8×10^5
	25	23 ± 8	7.9 ± 0.1	3.4×10^5
	40	54 ± 9	17.5 ± 0.2	3.3×10^5
***Mm*PFK/GK**	10	54 ± 7	5.1 ± 0.5	9.4×10^4
	25	62 ± 8	13.0 ± 0.8	2.1×10^5
	40	69 ± 9	27.0 ± 0.5	3.9×10^5

Table S3. Thermodynamic activation parameters for the psychrophilic *Mb*PFK/GK and the mesophilic *Mm*PFK/GK at different temperatures.

Enzyme	E_a, kcal mol^{-1}	T, °C	$\Delta G^{\ddagger}$, kcal mol^{-1}	$\Delta H^{\ddagger}$, kcal mol^{-1}	$T\Delta S^{\ddagger}$, kcal mol^{-1}
***Mb*PFK/GK**	10.3 ± 0.2	10	16.0	9.7	-6.3
		25	16.2	9.7	-6.5
		40	16.6	9.7	-6.9
***Mm*PFK/GK**	10.5 ± 0.1	10	15.6	9.9	-5,7
		25	15,8	9.9	-5.9
		40	16.3	9.9	-6.4

Table S4. Thermodynamic parameters for the temperature-dependent interaction of F6P with the active site of the psychrophilic *Mb*PFK/GK, the mesophilic *Mm*PFK/GK, the psychrophilic *Mb*PFK/GK quadruple mutant and the psychrophilic *Mb*PFK/GK double mutant.

Region	$\Delta S°$, kcal mol^{-1} K^{-1}	$\Delta H°$, kcal mol^{-1}
Mb (10°C-20°C)	-0.01281	-2.18196
Mb (20°C-40°C)	-0.04534	-11.72952
Mm	-0.01317	-1.49114
Mut4	-0.01312	-3.16602
Mut2 (15°C-	-0.02241	-4.86882

35°C)		
Mut2 (35°C-40°C)	-0.0472	-12.3651

Mb= psychrophilic *Mb*PFK/GK
Mm= mesophilic *Mm*PFK/GK
Mut4= psychrophilic *Mb*PFK/GK quadruple mutant
Mut2= psychrophilic *Mb*PFK/GK double mutant

Table S5. Amino acid residues of the active site of the psychrophilic *Mb*PFK/GK and the mesophilic *Mm*PFK/GK (5Å).

Enzyme	***Mb*PFK/GK**	***Mm*PFK/GK**
Active Site (total, 5Å)	41	36
Polar positively charged	5	4

Polar Negatively charged	5	5
Polar uncharged	9	11
Aromatics	2	0
Non-Polar	20	16

Table S6. Sequences of the 35 selected residues from the HDXMS experiments in the psychrophilic *Mb*PFK/GK.

Sequence	Peptide Mass (m/z) (Da)	No. of Amides	Region of *Mb*PFK/GK*	Region of *Mb*PFK/GK**
SSLDNVKGMF	1097.5296	9	19-28	19-28
VAYNSNIDAIKHVSEEDISM	2235.0598	19	29-48	29-44, 46-49

LLAQVDQNEVQDKL	1612.8541	13	49-62	50-63
FEYPRQIDSPSDLM	1697.7839	11	63-76	64-77
IIAMRDGKAAEVPTNTTDIHE	2282.1445	19	80-100	81-101
WLTDHLGFDNA	1288.5957	10	101-111	102-112
RMGGQAGIISNL	1216.6467	11	112-123	113-124
LASIGQN	702.3781	6	124-130	125-129, 131-132
VITYVPWLSAEQAE	1605.8159	12	131-144	133-146
YFVDSDNLLF	1232.5834	9	145-154	147-156
PVVEGDQL	856.4411	7	155-162	157-64
RLVRPRDAYDPQNKSKVNWIL	2568.4157	18	163-183	165-185
EFSKGMGVNF	1115.5190	9	184-193	186-195
KGEHFIVPRDNRL	1580.8656	11	194-206	196-208
IISSRPKW	986.5782	6	207-214	209-216
IRIEMVPEL	1099.6180	7	215-223	217, 219-226
YERIPSLQA	1076.5735	7	224-232	227-235
NIDGALL	715.3985	6	233-239	236-242
AGYQMIKEKYEDGSTYM	2013.8932	16	240-256	243-259
YMDYIDKAVNV	1330.6348	10	255-265	258-268
IERLKEGNPNIRIHVEF	2064.1349	15	266-282	269-285
TSIQNKLIRQSIL	1513.9061	12	283-295	286-298
KYIVKKHVHSLGLDTVE	1966.1120	16	296-312	299-315
NVLGYEE	823.3832	6	318-324	321-327
LAYSVINKGENAIVSL	1690.9374	15	325-340	328-343
FEGAVKLLKELEL	1488.8672	12	341-353	344-355, 357
ERVHVHSLGF	1180.6222	9	354-363	358-367
ICVVAKDCPVSVL	1345.7218	11	365-377	369-381
FASTTAASQAL	1067.5368	10	385-395	389-399
LGEIVSL	730.4345	6	396-402	400-406
ESTVAGLDVPVSDKGHGDLGRLED	2466.2107	22	403-426	407-430
MEDFENGCIRTPQYDA	1888.7840	14	436-451	440-455
IVIPTKVVSEPVAT	1452.8672	11	452-465	456-469
VGIGDVISA	830.4618	8	466-474	470-478
AGFLSKLK	863.5349	7	478-485	482-489

At least each residue in the table was present in two of three replicates; *Residue numbering is based on the original enzyme sequence; **Residue numbering is based on the alignment of the sequences shown in Figure S3.

Table S7. *S*equences of the 35 selected residues from HDXMS experiments in the mesophilic *Mm*PFK/GK.

Peptide Sequence	Peptide Mass (m/z) (Da)	No. of Amides	Region of *Mm*PFK/GK*	Region of *Mm*PFK/GK**
EIINHFKDFSNVSIF	1809.9170	14	02-16	13-25, 27-28

LAYNVNVDALKYLTDLSD	2027.0332	17	17-34	29-46
LKENFSDSEIKTKIEEYPRT	2427.2402	18	38-57	50-69
IEKPIDF	861.4716	5	58-64	70-76
VARLIHAMKSGKPAEVPLKNNL	2386.3751	19	65-86	77-98
FLNRLTYNE	1169.5949	8	91-99	103-111
ERIGGQVGIISNL	1355.7641	12	100-112	112-124
LSILNLKKIIF	1301.8555	10	113-123	125-135
YSPILAKKQAEM	1378.7399	10	124-135	136-147
FENNENLVF	1125.5211	8	136-144	148-156
PNITNGKL	856.4887	7	145-152	157-164
VLKKPIESFKNDEL	1659.9316	12	153-166	165-175, 177-179
KINRIFE	919.5360	6	167-173	180-186
YKEDIEF	943.4407	6	174-180	187-193
YLENEKITTPQSNRF	1839.9236	13	181-195	194-208
IVASRPENL	998.5629	7	196-204	209-217
RIEIKDEL	1015.5782	7	205-212	219-226
KSHLPEIGQLVD	1335.7267	10	213-224	227-238
CAIISGVQ	790.4128	7	225-232	239-246
AIKEEYSDGKTSE	1456.6802	12	233-245	247-259
YYLNKVKEDIKSLKKENKDLKVHFEF	3255.7776	25	246-271	260-285
ASIQNTEM	893.4033	7	272-279	286-293
RKKIAESIL	1057.6728	8	280-288	294-302
PEVDCVG	718.3076	6	289-295	303, 305-310
MDETEIANIIHVLG	1554.7832	13	296-309	311-324
YEELSEGILKHSKIEDVL	2102.1016	17	310-327	325-334, 337-344
KASKILL	772.5291	6	328-334	345-351
EKYNLEGMQVHTMYY	1905,8510	14	335-349	352-355, 357-367
YLCKKGGIL	994.5754	8	352-360	370-378
SDESLEKTLE	1150.5474	9	361-370	379-388
ASTKAALGQISS	1133.6161	11	376-387	394-405
IEDLKTGLKIPHNKHGEL	2042.1393	16	388-405	406-423
IVENISKEKELGG	1578.8374	13	409-422	427-430, 444-452
VPSRIVENPKSTVGLGDTISAGAF	2415.2878	21	427-450	458-481
VGYVSELKKLKNK	1505.9050	12	451-463	482-494

At least each residue in the table was present in two of three replicates; *Residue numbering is based on the original enzyme sequence; **Residue numbering is based on the alignment of the sequences shown in Figure S3.

Table S8. *S*equences of the 35 selected residues from HDXMS experiments in the psychrophilic *Mb*PFK/GK quadruple mutant

Peptide Sequence	Peptide Mass (m/z) (Da)	No. of Amides	Region of *Mb*PFK/GK*	Region of *Mb*PFK/GK**
SSLDNVKGMF	1097.5296	9	19-28	19-28
VAYNSNIDAIKHVSEEDISM	2235.0598	19	29-48	29-49
LLAQVDQNEVQDKL	1612.8541	13	49-62	50-63
FEYPRQIDSPSDLM	1697.7839	11	63-76	64-77
IIAMRDGKAAEVPTNTTDIHE	2282.1445	19	80-100	81-101
WLTDHLGFDE	1232.5582	9	101-110	102-111
ARMGGQAGIISNL	1287.6838	12	111-123	112-124
LASIGQN	702.3781	6	124-130	125-129, 131-132
VITYVPWLSAEQAE	1605.8159	12	131-144	133-146
FVDSDNLLF	1069.5201	8	146-154	148-156
PVVEGDQL	856.4411	7	155-162	157-164
RLVRPRDAYDPQNKSKVNWIL	2568.4157	18	163-183	165-185
EFSKGMGVNF	1115.5190	9	184-193	186-196
KGEHFIVPRDNRL	1580.8656	11	194-206	197-208
IISSRPKW	986.5782	6	207-214	209-216
IRIEMVPEL	1099.6180	7	215-223	217, 219-226
YERIPSLQA	1076.5735	7	224-232	227-235
NIDGALL	715.3985	6	233-239	236-242
AGYQMIKEKYEDGSTYM	2013.8932	16	240-256	243-259
YMDYIDKAVN	1231.5664	9	255-264	260-267
VIERLKEGNPNIRIHVEF	2163.2033	16	265-282	268-285
TSIQNKLIRQSIL	1513.9061	12	283-295	286-298
KYIVKKHVHSLGLDTVE	1966.1120	16	296-312	299-315
NVLGYEE	823.3832	6	318-324	321-327
LAYSVINKGENKIVDL	1775.9902	15	325-340	328-343
FEGAVKL	763.4349	6	341-347	344-350
ERVHVHSLGF	1180.6222	9	354-363	358-367
ICVVAKDCPVSVL	1345.7218	11	365-377	369-381
FASTTAASQAL	1067.5368	10	385-395	389-399
LGEIVSL	730.4345	6	396-402	400-406
ESTVAGLDVPVSDKGHGDLGRLED	2466.2107	22	403-426	407-430
EDFENGCIRTPQYDA	1757.7435	13	437-451	441-455
IVIPTKVVSEPKATVGIGDVISA	2293.3377	20	452-474	456-478
AGFLSKLK	863.5349	7	478-485	482-489

At least each residue in the table was present in two of three replicates; *Residue numbering is based on the original enzyme sequence; **Residue numbering is based on the alignment of the sequences shown in Figure S3.

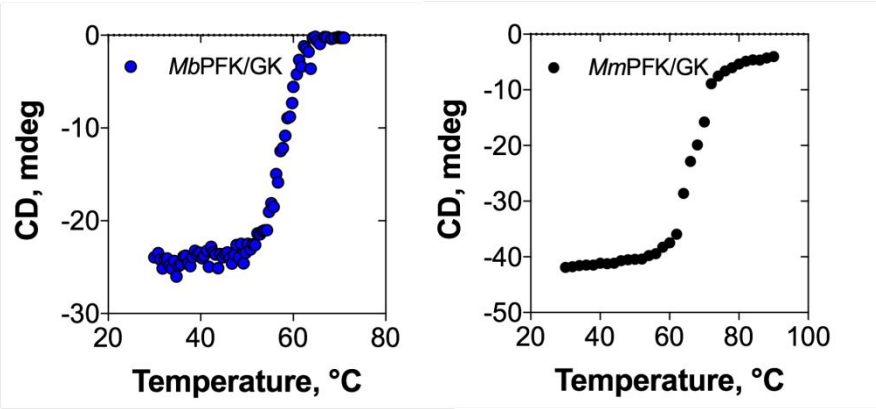

Figure S1. Raw data of the thermal unfolding of the psychrophilic *Mb*PFK/GK and the mesophilic *Mm*PFK/GK recorded by circular dichroism following the signal at 220 nm.

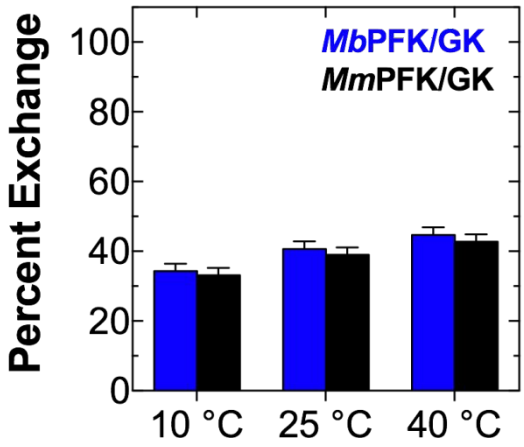

Figure S2. Average of the normalized deuterium uptake (amides) for all residues shown in Figure 2 from the psychrophilic *Mb*PFK/GK and the mesophilic *Mm*PFK/GK.

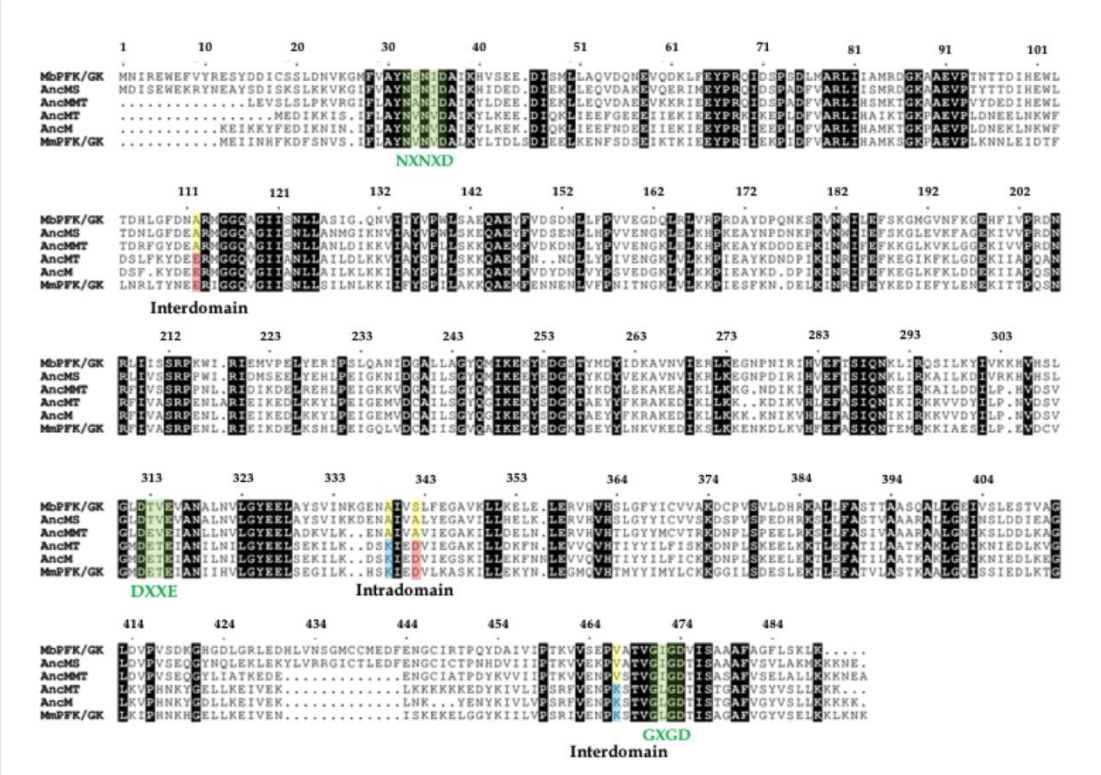

Figure S3. Structure-based multiple sequence alignment of extant and ancestral ADP-dependent kinases. Structure-based multiple sequence alignment was constructed based on three-dimensional and secondary structure constraints using Promals3D. The misaligned positions were corrected by visual inspection in Multiseq from VMD 1.9.3[9]. Red and blue blocks show the charged amino acids identified in this work, forming conserved ion pairs in the sequences of the mesophilic branch. Yellow blocks show amino acids found in the same positions but in the psychrophilic branch sequences. Green blocks show catalytic conserved motifs reported for the ADP-dependent sugar kinases family from archaea. Residue numbering is based on the psychrophilic *Mb*PFK/GK sequence considering sequence gaps.

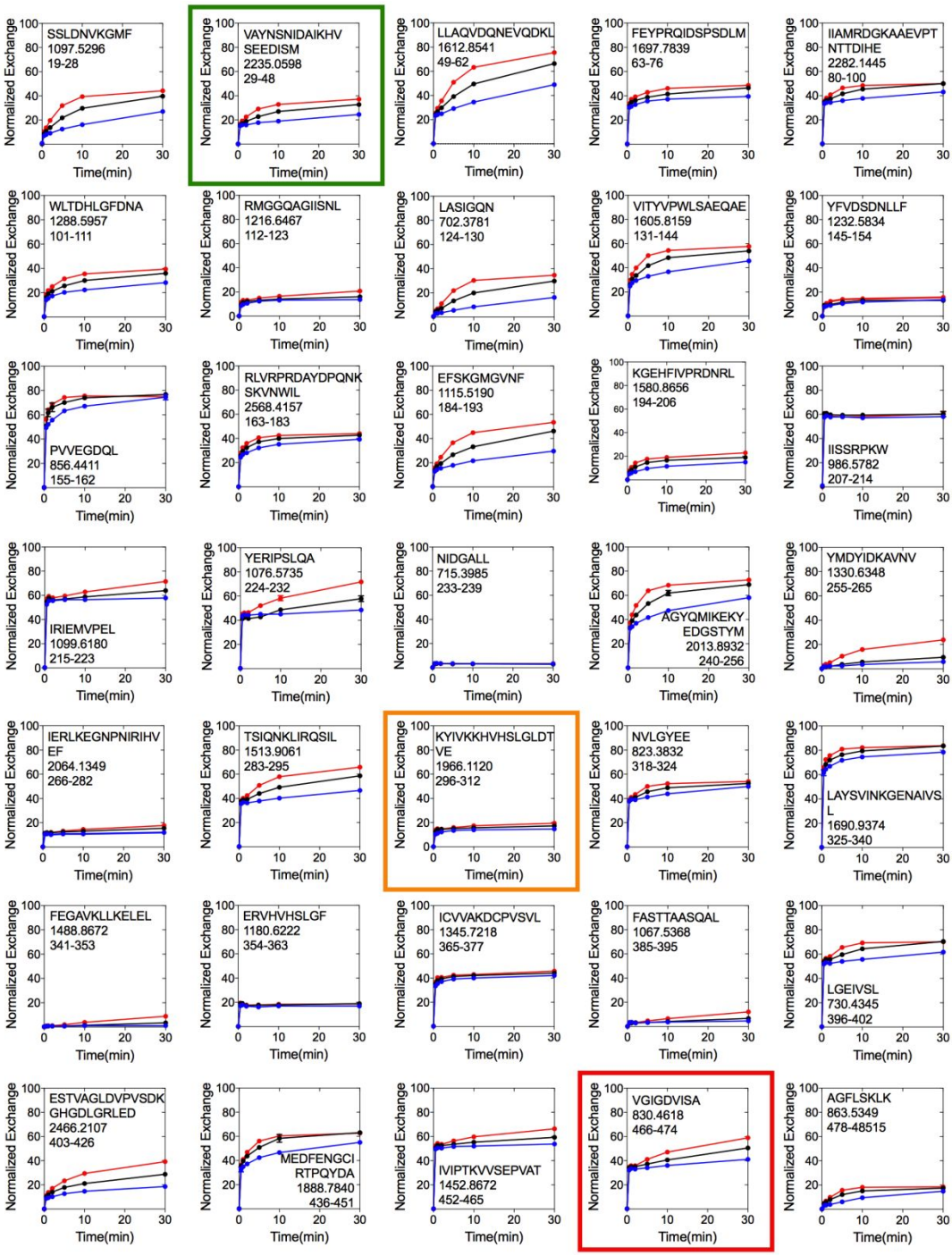

Figure S4. Deuterium uptake plots of the psychrophilic *Mb*PFK/GK residues used in the HDXMS data analysis presented in Figure 2A. Residues containing conserved

catalytic motifs NXNXD, DXXE and GXGD are boxed in green, orange and red, respectively.

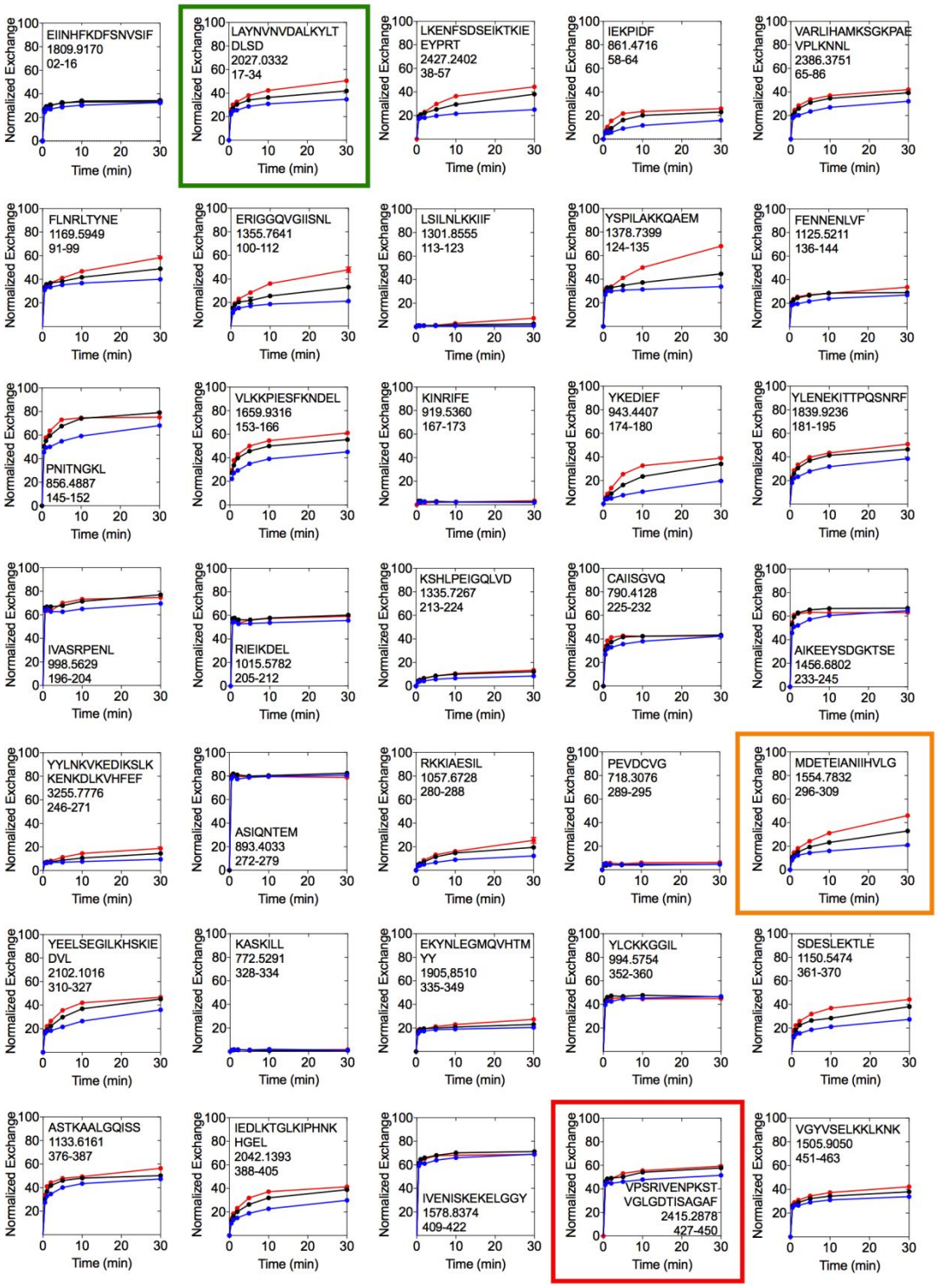

Figure S5. Deuterium uptake plots of the mesophilic *Mm*PFK/GK residues used in the HDXMS data analysis presented in Figure 2B. Residues containing conserved catalytic motifs NXNXD, DXXE and GXGD are boxed in green, orange and red, respectively.

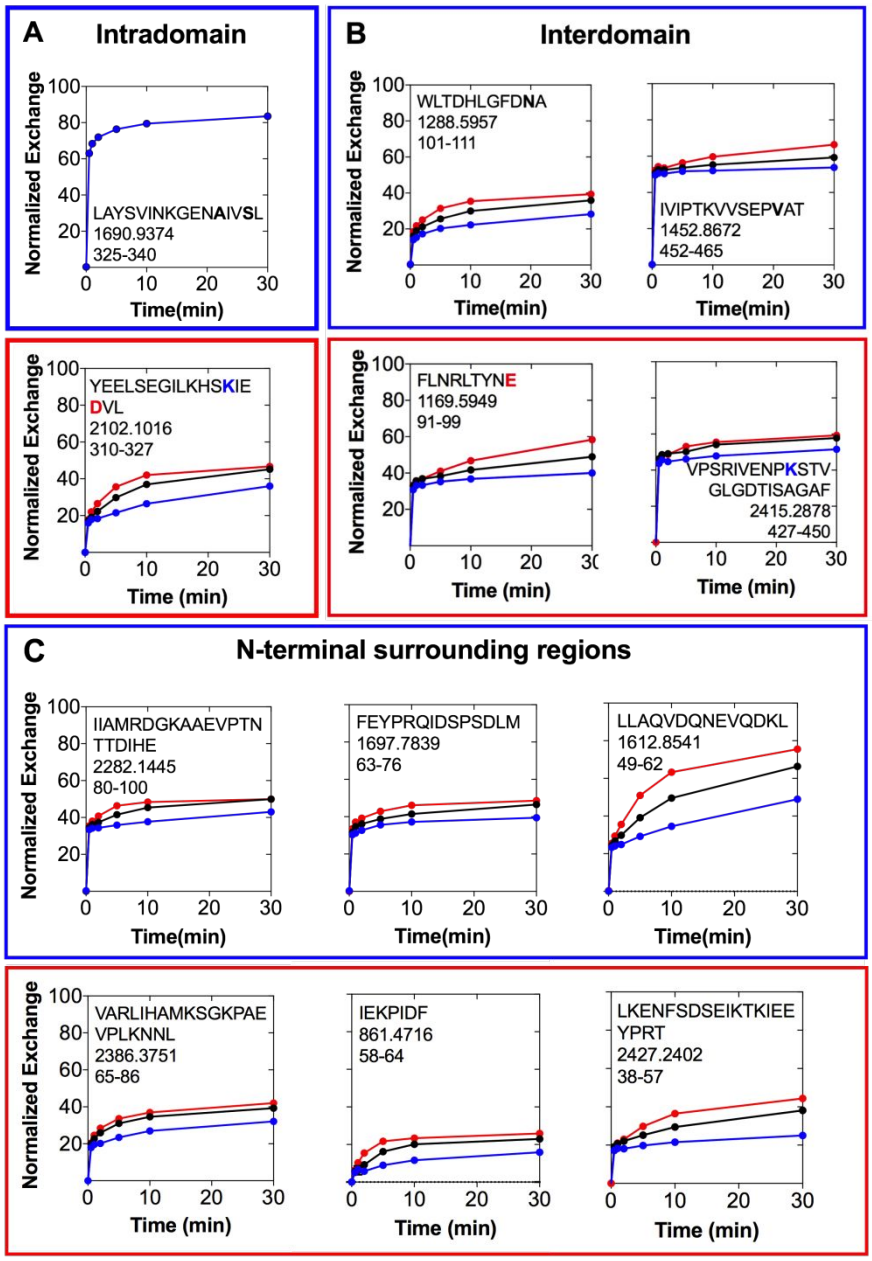

Figure S6. Comparison of the H/D exchange kinetics of residues involved in the intradomain (A) and interdomain (B) interactions in the psychrophilic *Mb*PFK/GK (blue blocks) and the mesophilic *Mm*PFK/GK (red blocks) at 10°C,

25°C, and 40°C. Panel C shows the H/D exchange variation of the N-terminal residues immediately contiguous to the segment containing the N110E variation in the mesophilic *Mm*PFK/GK. Residues contiguous to the segment containing the V463K variation in the mesophilic *Mm*PFK/GK are not shown because they did not differ significantly. H/D exchange differences were evaluated using a t-test with a p value cutoff of 0.05. Residue numbering shown in the uptake plots corresponds to the original position of the residues in each enzyme sequence.

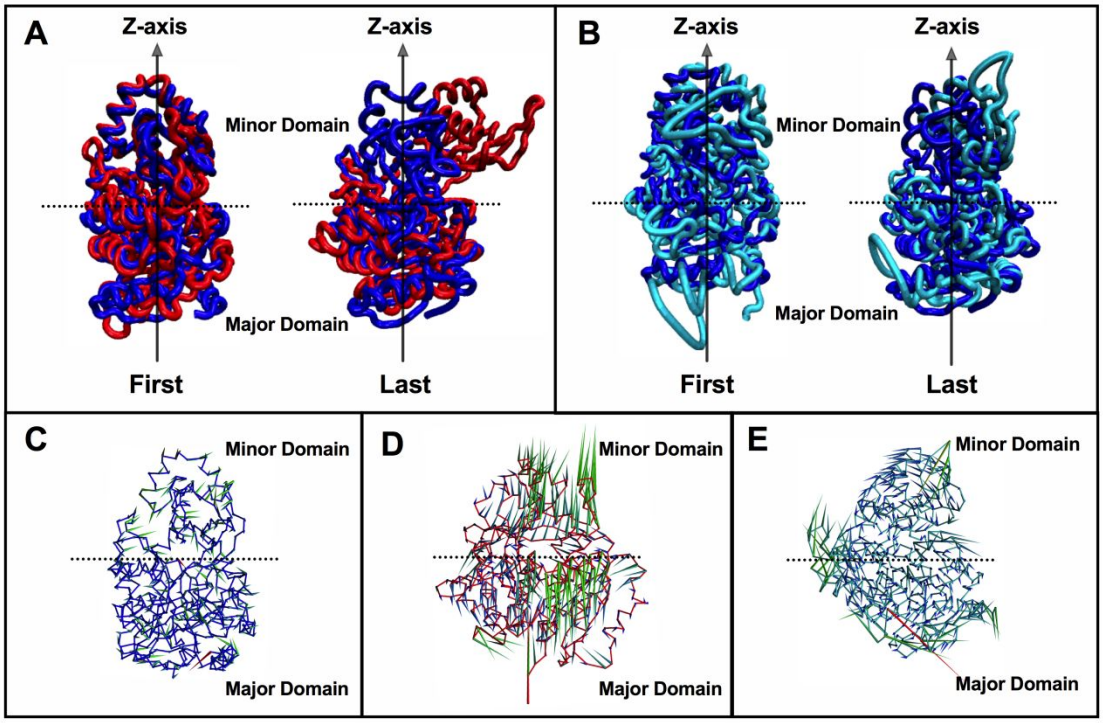

Figure S7. Representation of the trajectories obtained from the principal component analysis for the psychrophilic *Mb*PFK/GK, mesophilic *Mm*PFK/GK, and psychrophilic *Mb*PFK/GK quadruple mutant. A) Structural alignment (alpha-carbons) of the first and last frames of the principal component from psychrophilic *Mb*PFK/GK and the mesophilic *Mm*PFK/GK. B) Structural alignment (alpha-carbons) of the first and last frames of the principal component from psychrophilic *Mb*PFK/GK and psychrophilic

*Mb*PFK/GK quadruple mutant. C), D) and E): Trajectory representation of Principal Component 1 (PC1) of psychrophilic *Mb*PFK/GK, mesophilic *Mm*PFK/GK and psychrophilic *Mb*PFK/GK quadruple mutant, respectively. An arrowhead was drawn from the alpha-carbons of first frame to the last one for each enzyme using a Tcl/TK script (porcupine plot) available for VMD 1.9.3[9].

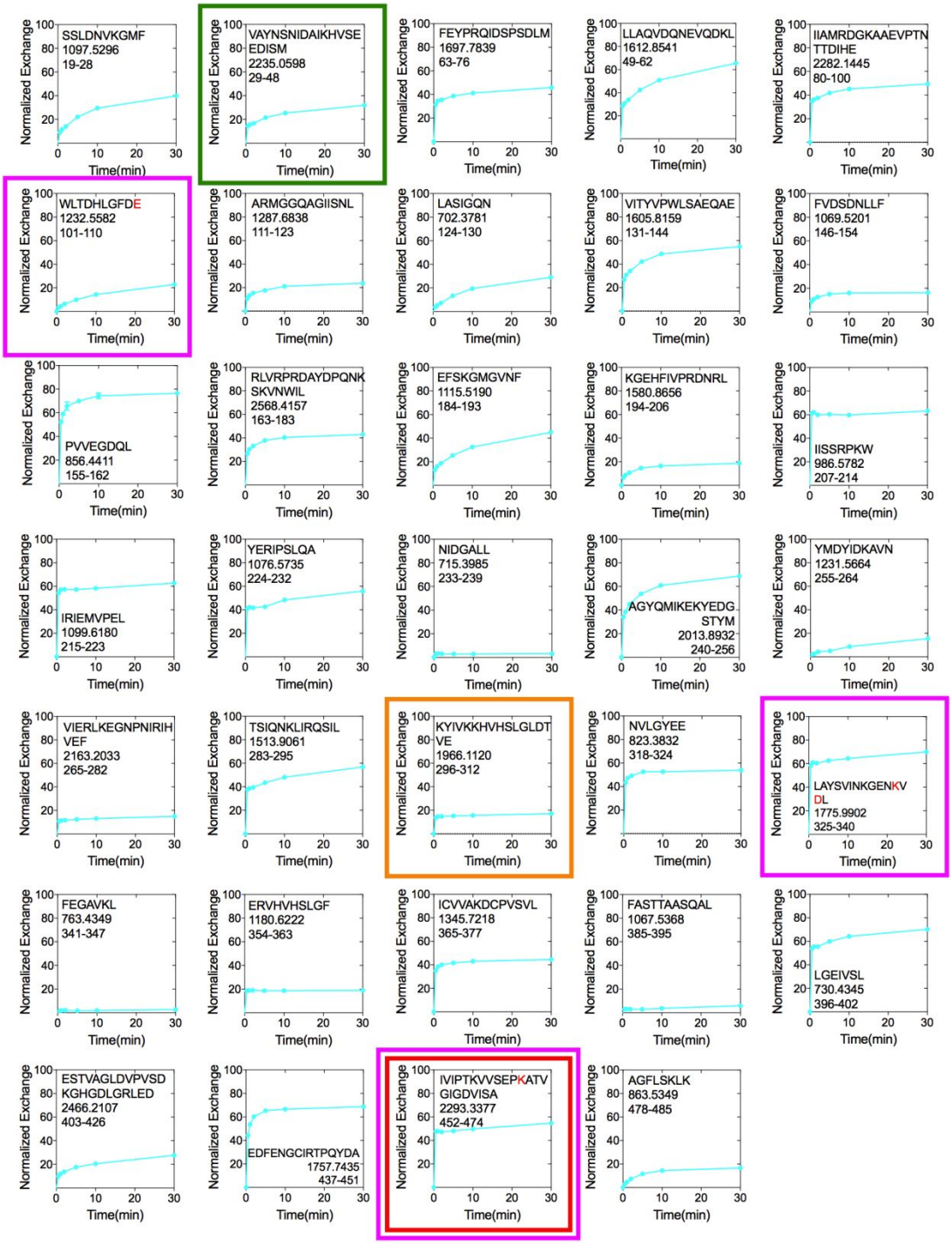

Figure S8. Deuterium uptake plots of the psychrophilic *Mb*PFK/GK quadruple mutant residues used in the HDXMS data analysis presented in Figure 6D. Residues containing conserved catalytic motifs NXNXD, DXXE and GXGD are boxed in green, orange and red, respectively. residues containing N110E, V463K, A336K and S339D mutations are boxed in magenta.

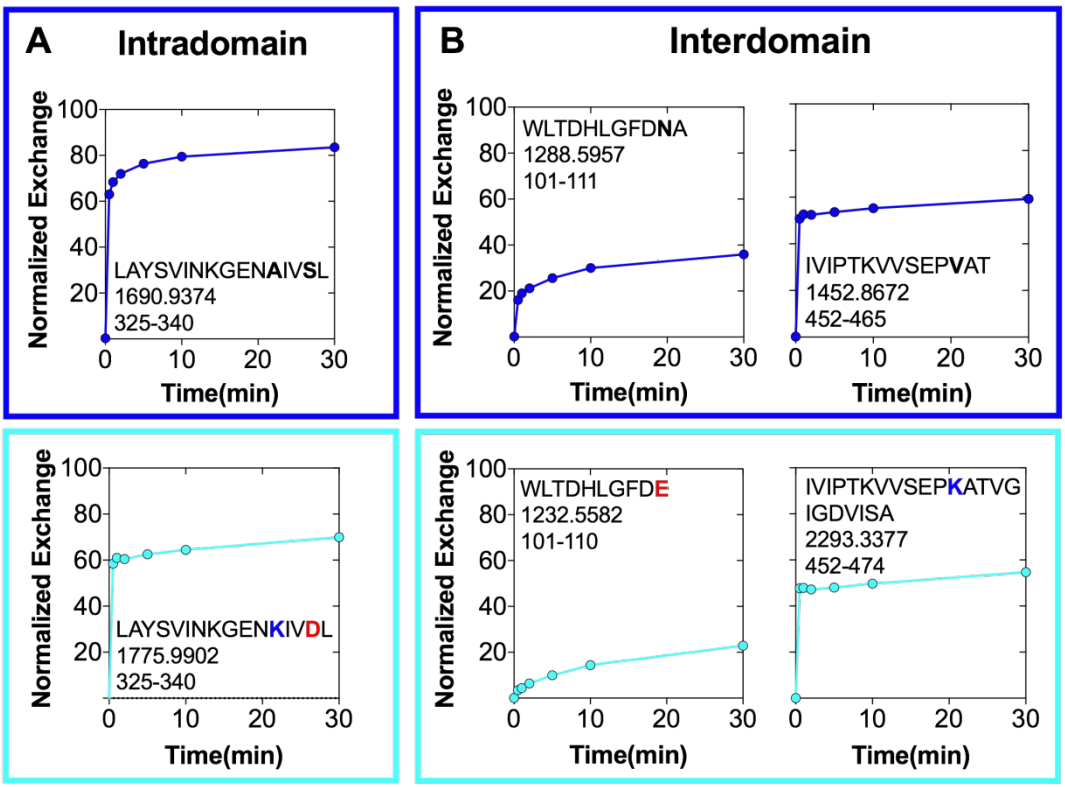

Figure S9. Comparison of the H/D exchange kinetics of the residues involved in the intradomain (A) and interdomain (B) interactions in the psychrophilic *Mb*PFK/GK (blue blocks) and the psychrophilic *Mb*PFK/GK quadruple mutant (cyan blocks) at 25°C. Residues contiguous to the segment containing the E110N and the V463K mutations in the psychrophilic *Mb*PFK/GK quadruple mutant, are not shown because they did not significantly differ. H/D exchange differences were evaluated using a t-test with a p value cutoff of 0.05.

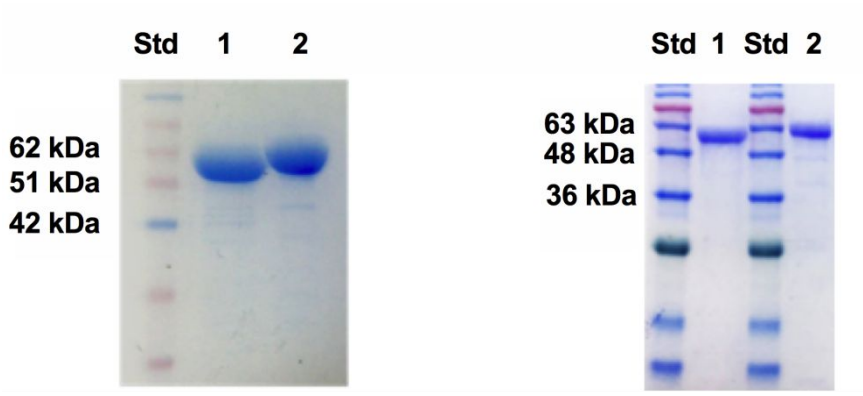

Figure S10. SDS-PAGE of the purification of the wild type and mutants ADP-dependent sugar kinases. Left panel show SDS-PAGE for the psychrophilic *Mb*PFK/GK (line 1) and psychrophilic *Mb*PFK/GK quadruple mutant (line 2). Right panel show SDS-PAGE for the mesophilic *Mm*PFK/GK (line 1) and psychrophilic *Mb*PFK/GK double mutant (line 2).

REFERENCES

(1) Zamora, R. A.; Gonzalez-Órdenes, F.; Castro-Fernández, V.; Guixé, V. ADP-Dependent Phosphofructokinases from the Archaeal Order *Methanosarcinales* Display Redundant Glucokinase Activity. *Arch. Biochem. Biophys.* **2017**, *633*, 85–92. https://doi.org/10.1016/j.abb.2017.09.008.
(2) Andrej Šali. MODELLER A Program for Protein Structure Modeling. *Comp. protein Model. by Satisf. Spat. restraints.* **1993**, *234* (3), 779-815. https://doi.org/10.1006/jmbi.1993.1626.
(3) Wiederstein, M.; Sippl, M. J. ProSA-Web: Interactive Web Service for the Recognition of Errors in Three-Dimensional Structures of Proteins. *Nucleic Acids Res.* **2007**, 35, W407-W410. https://doi.org/10.1093/nar/gkm290.
(4) Eisenberg, D.; Lüthy, R.; Bowie, J. U. VERIFY3D: Assessment of Protein Models with Three-Dimensional Profiles. *Methods Enzymol.* **1997**, *277*, 396-404. https://doi.org/10.1016/S0076-6879(97)77022-8.
(5) Castro-Fernandez, V.; Bravo-Moraga, F.; Herrera-Morande, A.; Guixe, V. Bifunctional ADP-Dependent Phosphofructokinase/Glucokinase Activity in the Order *Methanococcales* - Biochemical Characterization of the Mesophilic Enzyme from *Methanococcus Maripaludis*. *FEBS J.* **2014**, *281* (8), 2017–2029. https://doi.org/10.1111/febs.12757.
(6) Phillips, J. C.; Braun, R.; Wang, W.; Gumbart, J.; Tajkhorshid, E.; Villa, E.; Chipot, C.; Skeel, R. D.; Kale, L.; Schulten, K. Scalable Molecular Dynamics with NAMD. *J. Comput. Chem.* **2005**, *26* (16), 1781–1802.
(7) Huang, J.; Rauscher, S.; Nawrocki, G.; Ran, T.; Feig, M.; De Groot, B. L.; Grubmüller, H.; MacKerell, A. D. CHARMM36m: An Improved Force Field for Folded and Intrinsically Disordered Proteins. *Nat. Methods* **2016**, *14* (1), 71-73. https://doi.org/10.1038/nmeth.4067.
(8) Glykos, N. M. Carma: A Molecular Dynamics Analysis Program. *J Comput Chem* **2006**, *27* (14), 1765-8. https://doi.org/10.1002/jcc.
(9) Humphrey, W.; Dalke, A.; Schulten, K. VMD: Visual Molecular Dynamics. *J. Mol. Graph.* **1996**, *14* (1), 33-

28. https://doi.org/10.1016/0263-7855(96)00018-5.
(10) Willard, L.; Ranjan, A.; Zhang, H.; Monzavi, H.; Boyko, R. F.; Sykes, B. D.; Wishart, D. S. VADAR: A Web Server for Quantitative Evaluation of Protein Structure Quality. *Nucleic Acids Res.* **2003**, *31* (13), 3316–3319. https://doi.org/10.1093/nar/gkg565.
(11) Piovesan, D.; Minervini, G.; Tosatto, S. C. E. The RING 2.0 Web Server for High Quality Residue Interaction Networks. *Nucleic Acids Res.* **2016**, *44* (W1), W367-W374. https://doi.org/10.1093/nar/gkw315.